

# Geometric Scaling of Bayesian Inference in LLMs

Paper III of the Bayesian Attention Trilogy

NAMAN AGARWAL\*, Dream Sports, USA

SIDDHARTHA R. DALAL, Columbia University, USA

VISHAL MISRA, Columbia University, USA

Paper I establishes that neural sequence models can implement exact Bayesian inference when they realize the required *inference primitives*: belief accumulation, belief transport, and random-access binding. Paper II shows that gradient descent learns these primitives through dynamics exhibiting a mechanistic analogy to EM, sculpting a characteristic geometry—low-dimensional value manifolds and progressively orthogonal keys. We investigate whether this geometric substrate persists in production-grade language models. Across Pythia, Phi-2, Llama-3, and Mistral families, we find that last-layer value representations organize along a single dominant axis whose position strongly correlates with predictive entropy, and that domain-restricted prompts collapse this structure into the same low-dimensional manifolds observed in wind-tunnel settings. This suggests that the geometric mechanisms underlying the inference primitives are preserved at scale. To probe the role of this geometry, we perform targeted interventions on the entropy-aligned axis of Pythia-410M during in-context learning. Removing or perturbing this axis selectively disrupts the local uncertainty geometry, whereas matched random-axis interventions leave it intact. However, these single-layer manipulations do not produce proportionally specific degradation in Bayesian-like behavior, indicating that the geometry is a privileged *readout* of uncertainty rather than a singular computational bottleneck. Taken together, our results show that modern language models preserve the geometric substrate that underlies the inference primitives, and organize their approximate Bayesian updates along this substrate.

## 1 Introduction

Large language models have achieved striking performance across natural language, coding, mathematics, and reasoning tasks [5, 6, 12]. Yet their internal computations remain only partially understood. A central question is whether transformers merely approximate statistical associations at scale, or whether they implement more principled forms of probabilistic inference.

*Wind-tunnel results.* Paper I of this trilogy decomposes Bayesian inference into three *inference primitives*: belief accumulation (integrating evidence into a running posterior), belief transport (propagating beliefs through stochastic dynamics), and random-access binding (retrieving hypotheses by content). Different architectures realize different subsets: Transformers realize all three; Mamba realizes accumulation and transport; LSTMs realize only accumulation of static sufficient statistics; MLPs realize none. This taxonomy explains empirical performance across tasks. Paper II shows that gradient descent learns to implement these primitives through dynamics exhibiting a mechanistic analogy to EM, sculpting a characteristic geometry: value manifolds ordered by entropy, orthogonal key frames defining hypothesis directions, and layerwise attention sharpening implementing a geometric Bayes rule. These findings established that transformers *can* implement Bayesian inference when trained on tasks with known posteriors, and identified the geometric substrate that supports the inference primitives. What remains open is whether the same geometric mechanisms persist in large, naturally trained LLMs, where ground-truth posteriors are unavailable.

\*Currently at Google DeepMind. Work performed while at Dream Sports.

*The central question.* This paper asks: *Do the geometric structures that enable exact Bayesian inference in wind tunnels persist in production-scale language models?* We do not claim that LLMs compute true Bayesian posteriors for natural language. Instead, we evaluate whether they preserve the same representational and computational geometry - value manifolds, key orthogonality, and attention focusing - that underpins Bayesian inference in controlled settings.

*Clarification on “Bayesian inference.”* Throughout this trilogy, “Bayesian inference” refers to the *Bayesian posterior predictive over latent task variables*—e.g., filtering posteriors over hidden states—not a posterior over network weights. This is a statement about the function the transformer computes, not about weight-space uncertainty. Several factors make this question non-trivial:

- natural language lacks tractable ground-truth posteriors;
- production models employ architectural optimizations (GQA, RoPE, sliding-window attention) absent from wind-tunnel setups;
- web-scale training introduces noise that may obscure geometric structure;
- large models may develop new mechanisms not visible at small scale.

*Our approach.* Rather than attempting to define Bayesian posteriors for natural language, we test whether the *geometric substrate* identified in Papers I–II persists across architectures and training regimes. We treat these geometric signatures as invariants: if transformers rely on similar computational principles at scale, the same value–key–attention geometry should appear even when exact posteriors cannot be measured.

*Three main findings.* First, **domain restriction produces a decisive bridge.** Under mixed-domain prompts, value manifold dimensionality varies substantially across architectures (PC1+PC2 ranging from ~15% in Mistral to ~99% in Pythia-410M), reflecting different inductive biases and training regimes. However, *single-domain prompts consistently collapse the manifold toward one dimension* (PC1+PC2  $\approx$  70–95%), approaching the geometric regime observed in wind-tunnel experiments. This collapse shows that production LLMs contain the same entropy-ordered Bayesian axis that wind-tunnel transformers learn explicitly. Second, **Bayesian updating persists at inference time.** In a controlled in-context learning experiment (SULA), models move smoothly along their value manifold as more evidence is supplied, and manifold coordinates correlate strongly with analytical Bayesian entropy. This demonstrates that the geometry is not merely a training artifact - it is used during inference. Third, **static and dynamic geometric signatures separate cleanly.** Value manifolds and key orthogonality are universal across architectures, including sliding-window and MoE variants. Dynamic attention focusing, however, depends on routing capacity: strong in full-sequence MHA, moderate in GQA, and weak or noisy in Mistral. This matches the frame–precision dissociation predicted in Paper II.

*Relation to prior work.* Paper I established *which* architectures can implement Bayesian inference, taxonomized by three inference primitives (belief accumulation, belief transport, random-access binding). Paper II showed *how* gradient dynamics learn to implement these primitives through mechanisms exhibiting a mechanistic analogy to EM, sculpting characteristic geometric structures. However, these results were obtained in synthetic domains with analytically specified likelihoods. The present work answers a distinct question: *do production-grade LLMs, trained on heterogeneous natural language, spontaneously develop the same geometric signatures that underlie the inference primitives?* We show that the three hallmarks of Bayesian geometry—low-dimensional value manifolds, orthogonal hypothesis frames, and evidence-dependent movement along entropy-aligned directions—persist across four model families (Pythia, Phi-2, Llama-3, Mistral). Moreover, we provide the first large-scale evidence that these structures are *functionally engaged* during inference in a

naturalistic task (SULA), even when their causal role is distributed rather than bottlenecked. This establishes that the geometric substrate for the inference primitives is a stable inductive bias of modern transformers, not an artifact of synthetic tasks.

*Contributions.* This paper makes four contributions:

- (1) **Persistence of Bayesian geometry at scale.** We show that production LLMs exhibit the same value-manifold structure, key orthogonality, and domain-specific collapse previously identified in wind-tunnel settings, confirming that these geometric signatures are not artifacts of synthetic tasks or toy models.
- (2) **Functional alignment with posterior uncertainty.** In structured uncertainty-learning-from-examples (SULA) tasks, model states move systematically along entropy-aligned manifold directions as prompt evidence increases, and manifold position correlates with analytically computed posteriors.
- (3) **Domain-restriction bridge.** When prompts are restricted to a coherent domain, the value manifold collapses to one or two principal components explaining 80–95% of variance, numerically matching the geometric regime predicted by Paper I and derived in Paper II.
- (4) **Causal boundary characterization.** Targeted interventions on the entropy-aligned axis selectively destroy the local geometry but do not proportionally disrupt Bayesian-like calibration, establishing that the geometry is representationally privileged yet not behaviorally singular, and identifying distributed uncertainty representation as a key direction for future work.

## 2 Background: Bayesian Geometry in Controlled Settings

Papers I–II established that small transformers trained in controlled “Bayesian wind-tunnel” settings perform near-exact Bayesian inference on tasks with analytically tractable posteriors. We summarize only the key findings needed for the production-model analysis; full experimental details appear in those papers.

*Bayesian tasks.* Two families of synthetic tasks provided ground-truth posteriors: (1) **Bijection learning** (Paper I): models infer a random bijection  $\pi : V \rightarrow W$  from in-context examples. Because the hypothesis space has size  $K!$  (e.g.,  $3.6 \times 10^6$  for  $K = 10$ ), memorization is impossible; exact analytic posterior trajectories are available. Transformers achieve MAE  $< 0.1$  bits between model and Bayes-optimal predictive entropy. (2) **HMM filtering** (Paper I): models track posterior distributions over latent states in Hidden Markov Models with  $S = 5$  states and  $V = 5$  emissions. Transformers match analytic posteriors with KL divergence  $< 0.05$  bits, including strong length generalization.

*Geometric structures.* Across both tasks, three geometric signatures emerged:

- **Value manifolds:** last-layer value vectors form low-dimensional trajectories parameterized by predictive entropy (PC1 explains 84–90%), providing a geometric encoding of posterior uncertainty.
- **Key orthogonality:** key matrices develop structured hypothesis-frame directions (mean off-diagonal cosine 0.09–0.12 vs. 0.40–0.45 random).
- **Attention-as-posterior:** attention weights align with analytic posteriors (KL  $\approx 0.05$  bits), implementing a geometric Bayes rule.

*Gradient mechanism.* Paper II showed that cross-entropy gradients generate this geometry via coupled specialization of queries, keys, and values. A predicted *frame-precision dissociation* emerges: attention patterns (the frame) stabilize early, while value manifolds (precision) continue refining.

*Forward pointer.* In this paper, we evaluate whether the static and dynamic geometric signatures identified in wind-tunnel models - entropy-ordered value manifolds, orthogonal hypothesis frames, and layerwise attention refinement - persist in production-scale LLMs and whether these structures are used during inference. Section 5 presents our empirical findings across architectures.

### 3 Hypotheses and Predictions

We formalize the geometric hypotheses tested in production models. These hypotheses capture geometric signatures that should be recoverable across architectures if transformers rely on similar uncertainty-representation mechanisms at scale. They do not assume that models compute exact posteriors on natural language, but that they preserve the geometric substrate supporting Bayesian-style inference.

#### 3.1 Core Hypotheses

*Hypothesis 3.1 (Value manifold persistence).* If transformers maintain Bayesian-style uncertainty representations at scale, last-layer value vectors should form low-dimensional manifolds parameterized by predictive entropy. Specifically:

- $PC_1$  should exceed random baselines (typically  $\sim 5\%$  for Gaussian vectors), with  $PC_1+PC_2$  in the range 20–40% under mixed-domain prompts and increasing sharply under domain restriction.
- Value coordinates should correlate with next-token entropy.
- Manifold dimensionality may vary by depth and architecture, reflecting richer uncertainty representations in deeper networks.

*Hypothesis 3.2 (Key orthogonality).* If keys encode hypothesis-frame directions, then key projection matrices should exhibit structured orthogonality:

- Early and mid layers should show lower mean off-diagonal cosine similarity than both random Gaussian baselines and initialization baselines.
- Orthogonality should weaken in final layers as the model commits to an output distribution.
- Training data quality should correlate with the strength of orthogonality.

*Hypothesis 3.3 (Attention focusing).* If attention implements evidence integration, attention entropy should decrease with depth:

- Layerwise entropy reduction should exceed  $\sim 30\%$  from input to output.
- Refinement should be progressive rather than abrupt where global routing is available.
- Architectural constraints (e.g., GQA, sliding-window attention) may attenuate the magnitude or monotonicity of focusing.

#### 3.2 Architectural Predictions

*Prediction 3.4 (Standard MHA).* Standard full-sequence MHA should exhibit the clearest geometric signatures, matching wind-tunnel architectures most closely.

*Prediction 3.5 (Grouped-query attention).* GQA should preserve qualitative Bayesian geometry but with weaker orthogonality and reduced focusing, as shared K/V heads must serve multiple query groups.

*Prediction 3.6 (Training data quality).* Curated, high-signal training data should enhance geometric clarity and improve both orthogonality and attention refinement.

*Prediction 3.7 (Depth and dimensionality).* Deeper models may develop multi-dimensional or multi-lobed manifolds under mixed prompting while still collapsing to one-dimensional structure under domain restriction.

## 4 Methods

### 4.1 Model Selection

We selected three production models to span architectural and training variations: **Pythia-410M** [4]: GPT-NeoX architecture, 24 layers, 16 attention heads, 1024 hidden dimensions. Trained on the Pile corpus (800GB diverse text) with full training transparency. Represents canonical standard MHA trained on general-purpose data. **Phi-2**: Microsoft Research model, 2.7B parameters, 32 layers, 32 attention heads, 2560 hidden dimensions. Standard MHA trained on curated textbook-quality and code data. Represents optimal training conditions for geometric clarity. **Llama-3.2-1B**: Meta model, 16 layers, 32 query heads, 8 key-value heads (4:1 grouped-query attention), 2048 hidden dimensions with rotary position embeddings. Trained on large-scale web data. Represents efficiency-optimized architecture for production deployment.

### 4.2 Geometric Extraction Protocol

We extract value manifolds, key orthogonality structure, and attention–entropy trajectories using a uniform protocol across all models. All forward passes use each model’s native tokenizer and positional–embedding scheme without modification.

*Prompt sampling.* To avoid selection bias, we adopt a reproducible stratified–entropy sampling procedure. We first generate 1,000 candidate prompts from five heterogeneous corpora (Wikipedia articles, news, fiction excerpts, code repositories, and general–knowledge QA). For each prompt we compute the model’s next–token entropy on the final position and partition the candidates into quintiles. We then uniformly sample 15 prompts per quintile (total 75 mixed–domain prompts). For domain–restricted experiments (e.g., mathematics, coding, philosophy), we filter the candidate pool to the relevant domain and apply the same stratified procedure. This ensures that geometric results do not depend on hand–chosen or manually curated prompts.

*Final-token extraction.* For a prompt of length  $T$ , we perform a single forward pass and extract geometric quantities from the representations associated with the final input token. Specifically, for each layer  $\ell$  we extract:

- (1) value vectors  $v_{T,h}^{(\ell)} \in \mathbb{R}^{d_v}$  from all attention heads  $h$ ,
- (2) the key projection matrix  $W_K^{(\ell)} \in \mathbb{R}^{d_{\text{model}} \times d_k}$ ,
- (3) the attention distribution  $\alpha_{T,h}^{(\ell)} \in [0, 1]^T$  for each head at query position  $T$ ,
- (4) the next–token probability distribution  $p(x_{T+1} | x_{1:T})$ .

The final-token choice ensures that the extracted geometry reflects the model’s posterior uncertainty after processing the entire prompt.

*Value manifold computation.* For each model, we adopt a canonical PCA protocol on the final-layer value space. For a prompt of length  $T$ , we extract the V-projection outputs  $v_{T,h}^{(L)} = W_V^{(h)} x_T \in \mathbb{R}^{d_v}$  for the final input token  $T$  at the last layer  $L$  from all attention heads  $h = 1, \dots, H$ . We then concatenate the head-wise values into a single vector  $\tilde{v}_T^{(L)} \in \mathbb{R}^{Hd_v}$  per prompt, so that each prompt contributes one  $Hd_v$ -dimensional sample. Before PCA, we standardize each coordinate across the prompt batch to zero mean and unit variance. All reported  $\text{PC}_1$  and  $\text{PC}_1 + \text{PC}_2$  statistics are computed from this standardized covariance matrix, separately for mixed-domain and domain-restricted prompt sets.

Unless otherwise noted, PCA is run independently per model and per layer; cross-model analyses in Section 5.8 use a global PCA basis constructed by concatenating standardized value vectors across models.

*Effective dimensionality (participation ratio).* To complement  $PC_k$  explained-variance ratios, we report the *participation ratio* (PR) as a continuous measure of effective dimensionality. Let  $\{\lambda_i\}$  denote the eigenvalues of the standardized covariance matrix in descending order. The participation ratio is

$$PR = \frac{\left(\sum_i \lambda_i\right)^2}{\sum_i \lambda_i^2},$$

which equals the dimensionality for a perfectly isotropic spectrum and decreases as mass concentrates on a low-rank subspace. Low PR values co-occur with high  $PC_1+PC_2$  and provide an additional check that “manifold collapse” is not an artifact of preprocessing or finite-sample noise.

*Correct attention-entropy computation.* Because entropy is concave, averaging attention weights *before* computing entropy introduces a Jensen bias. We therefore compute attention entropy at the granularity of individual heads on the *final input token*  $T$ :

$$H_h^{(\ell)}(T) = -\sum_{j=1}^T \alpha_{T,h}^{(\ell)}(j) \log \alpha_{T,h}^{(\ell)}(j),$$

where  $\alpha_{T,h}^{(\ell)}$  denotes the attention distribution over keys for head  $h$  in layer  $\ell$ . We then average these entropies *only across heads* and report bootstrap 95% confidence intervals across prompts:

$$H^{(\ell)} = \frac{1}{H} \sum_{h=1}^H H_h^{(\ell)}(T).$$

This protocol aligns attention entropy with the value-vector geometry and predictive entropy at the same token, and avoids the Jensen bias that arises from averaging distributions prior to entropy computation.

*Key orthogonality.* For each layer  $\ell$  and head  $h$ , we take the key projection matrix  $W_K^{(\ell,h)} \in \mathbb{R}^{d_{\text{model}} \times d_k}$ , extract its  $d_k$  column vectors, and  $\ell_2$ -normalize each column to obtain unit vectors  $\{\hat{k}_i\}_{i=1}^{d_k} \subset \mathbb{R}^{d_{\text{model}}}$ . Note that we measure orthogonality of the learned parameter matrix columns, not token-conditioned key vectors; this captures the static geometric structure of the hypothesis frames established during training. We then compute the mean off-diagonal absolute cosine similarity

$$\text{Orthog}^{(\ell,h)} = \frac{1}{d_k(d_k - 1)} \sum_{i \neq j} |\hat{k}_i^\top \hat{k}_j|,$$

and report layer-wise means and percentile bands across heads. To interpret these values we use two baselines:

- *Gaussian baseline.* If  $\hat{k}_i, \hat{k}_j$  were independent random unit vectors in  $\mathbb{R}^{d_{\text{model}}}$ , the expected absolute cosine would be  $\mathbb{E}[|\cos \theta|] \approx \sqrt{2/(\pi d_{\text{model}})}$ . For  $d_{\text{model}}$  in the 1024–4096 range, this lies between 0.02 and 0.04 and provides the correct dimensionality-matched reference.
- *Initialization baseline.* For models with public initialization checkpoints (e.g., Pythia), we measure  $\text{Orthog}^{(\ell,h)}$  at training step 0. These empirical values fall around 0.35–0.45, reflecting correlations induced by initialization schemes and architectural shared structure rather than i.i.d. Gaussian randomness.

Trained models consistently achieve mean off-diagonal cosines between 0.034 and 0.18 across most layers, representing a 2–10× improvement relative to the initialization baseline and confirming that training sculpts sharper hypothesis frames than either Gaussian or initialization structure would predict.

*Cross-model PCA analysis.* For comparisons across architectures, we standardize all value vectors per model (zero mean, unit variance per dimension), concatenate them, and compute a global covariance matrix. This enables interpretation of shared manifold directions and consistent alignment of entropy-ordered axes across models.

### 4.3 In-Context Bayesian Updating Task

To test whether production models perform Bayesian updating during inference, we designed a controlled in-context learning task. Each prompt contains  $k$  labeled sentiment examples (e.g., “happy is positive”, “sad is negative”) followed by a query word. We compute analytical Bayesian posteriors using a Beta-Bernoulli model with uniform Beta(1,1) prior and likelihood ratio 0.9:0.1 for consistent vs. inconsistent labels, generating 250 prompts across  $k \in \{0, 1, 2, 4, 8\}$  with varying label imbalances. SULA is not intended as a model of natural-language reasoning, but as a controlled probe isolating Bayesian updating from linguistic ambiguity.

### 4.4 Validation Criteria

We establish quantitative thresholds for Bayesian structure validation based on wind tunnel experiments:

- **Value manifolds:**  $PC1 > 30\%$  or  $PC1+PC2 > 30\%$  (vs. 5% baseline for random)
- **Key orthogonality:** Mean off-diagonal  $< 0.20$  for at least 50% of layers
- **Attention focusing:**  $> 30\%$  entropy reduction from Layer 0 to final layer

Models meeting all three criteria exhibit Bayesian geometric signatures. Partial validation (2/3 criteria) suggests preserved qualitative structure with reduced clarity. **Threshold justification.** These thresholds are anchored to quantitative baselines from controlled wind-tunnel settings and random-initialization controls. In bijection and HMM tasks, trained models produce nearly one-dimensional value manifolds with  $PC1 = 84\text{--}90\%$  of variance explained. Under mixed-domain prompting in production models, multiple inference modes are simultaneously active, so we conservatively treat  $PC1+PC2$  values in the 20–40% range as non-trivial structure over the random baseline of  $\sim 5\%$  for  $PC1$ . When prompts are domain-restricted, all models recover the same collapsed geometry as in wind-tunnel tasks ( $PC1 \approx 0.75\text{--}0.85$ ;  $PC1+PC2 \approx 0.85\text{--}0.95$ ). For key orthogonality, random Gaussian  $W_K$  matrices yield mean off-diagonal cosine values around 0.40–0.45. Trained models consistently achieve 0.03–0.20 depending on layer depth, so we adopt  $< 0.20$  as a minimal criterion for structured hypothesis frames. Wind-tunnel attention mechanisms reduce entropy by 85–90%. Production models face more heterogeneous workloads and architectural constraints (e.g., GQA), therefore we use a lenient 30% threshold to require meaningful focusing without expecting full collapse. These thresholds are conservative: varying them within reasonable ranges does not change any model’s qualitative classification or the cross-model trends reported in this paper.

### 4.5 Statistical Validation

We evaluate the significance of geometric structure by comparing trained models against two distinct baselines: (i) a theoretically grounded high-dimensional Gaussian baseline, and (ii) each model’s own initialization (when available). These baselines separate geometry induced purely by dimensionality or initialization from structure learned during training.

*Value manifolds.* Under the null hypothesis that value vectors are random high-dimensional embeddings, the expected variance captured by the top principal component is  $\mathbb{E}[\text{PC}_1] \approx 1/d$  for  $d$ -dimensional Gaussian vectors (typically  $\approx 5\%$  for our head-concatenated value dimension). Across all models, observed  $\text{PC}_1$  values under mixed-domain prompts are 6–17 $\times$  larger, and domain-restricted prompts yield collapsed 1D manifolds ( $\text{PC}_1 \approx 0.75\text{--}0.85$ ,  $\text{PC}_1+\text{PC}_2 \approx 0.85\text{--}0.95$ ). These differences are statistically significant under paired  $t$ -tests across prompt batches ( $p < 0.001$  after Bonferroni correction).

*Key orthogonality.* We compare trained key matrices against two baselines:

- (1) **Gaussian baseline.** For  $d_k$ -dimensional random Gaussian vectors, the expected absolute cosine similarity is

$$\mathbb{E}[|\cos(\theta)|] = \sqrt{\frac{2}{\pi d_k}},$$

which equals  $\approx 0.11$  for  $d_k = 64$  and decreases with dimensionality. This provides the correct reference for high-dimensional orthogonality.

- (2) **Initialization baseline.** For models where initialization checkpoints are publicly available (e.g., Pythia), we measure the mean off-diagonal cosine similarity of  $W_K$  at step 0. These values (typically 0.35–0.45, depending on the initialization scheme) reflect correlations introduced by weight initialization rather than pure Gaussian randomness.

Trained models achieve mean off-diagonal cosine similarities between 0.034 and 0.18 across most layers - representing a 2–10 $\times$  improvement relative to the appropriate baselines. This confirms that training sculpts structured hypothesis frames rather than merely preserving initialization correlations.

*Attention entropy.* For each model, we compute per-head, per-position attentional entropies and average across heads and positions. Layerwise entropy reduction is evaluated relative to the entropy of the bottommost attention layer. All reductions exceeding 30% are significant under paired comparisons across prompts ( $p < 0.01$ ), and the architecture-dependent patterns (Section 5) are robust under bootstrap resampling.

*Multiple comparisons.* All hypothesis tests involving multiple layers, domains, or prompt buckets use a Bonferroni correction. All reported results remain significant at the  $p < 0.01$  level after correction.

*Entropy-axis definition and interventions.* For causal probes of the entropy-aligned manifold, we first estimate an “entropy axis”  $u_{\text{ent}}^{(\ell)}$  at each layer  $\ell$  by computing the first principal component of the standardized final-token value vectors across SULA prompts, and then taking the sign so that  $\text{corr}(v^{(\ell)} \cdot u_{\text{ent}}^{(\ell)}, H_{\text{model}})$  is non-negative. For a given intervention layer (or set of layers), we apply a projection-removal operator to the value vectors during the forward pass:

$$\tilde{v}^{(\ell)} = v^{(\ell)} - (v^{(\ell)} \cdot u_{\text{ent}}^{(\ell)}) u_{\text{ent}}^{(\ell)},$$

leaving all other components unchanged. “True-axis” interventions use  $u_{\text{ent}}^{(\ell)}$  as defined above; “random-axis” controls draw a unit vector from a Gaussian in  $\mathbb{R}^{Hd_v}$  and orthogonalize it against  $u_{\text{ent}}^{(\ell)}$  before applying the same projection operator. We report the impact of these interventions on (i) the correlation between  $v^{(\ell)} \cdot u_{\text{ent}}^{(\ell)}$  and model predictive entropy, and (ii) SULA calibration metrics (MAE and entropy correlation) relative to the unperturbed baseline.

#### 4.6 Causal Intervention Protocol: Entropy-Axis Ablations

For the causal probes in Section 6, we construct entropy-aligned axes and ablate them using a simple linear projection scheme.

*Axis estimation.* For each layer  $\ell$  of Pythia-410M we collect last-layer value vectors  $v_{T,h}^{(\ell)}$  for a held-out set of 200 SULA prompts (disjoint from the 300 evaluation prompts) and compute a layer-specific PCA basis as in Section 4.2. We take the first principal component  $u_{\text{ent}}^{(\ell)}$  and orient its sign so that the dot product  $v_{T,h}^{(\ell)} \cdot u_{\text{ent}}^{(\ell)}$  correlates *positively* with predictive entropy (i.e., high projection = high uncertainty); this defines the *entropy axis* for that layer. Interventions are then evaluated on the separate evaluation set to avoid overfitting. Random control axes  $u_{\text{rand}}^{(\ell)}$  are drawn by sampling a Gaussian vector in the same space and normalizing to unit norm.

*Single-layer axis cuts.* In the *axis-cut* intervention we remove the component of each value vector along a chosen axis,

$$\tilde{v}_{T,h}^{(\ell)} = v_{T,h}^{(\ell)} - \lambda (v_{T,h}^{(\ell)} \cdot u^{(\ell)}) u^{(\ell)},$$

with  $\lambda = 1$  for the hard-ablation experiments reported here. We apply this operation either along  $u_{\text{ent}}^{(\ell)}$  (“true” cut) or along  $u_{\text{rand}}^{(\ell)}$  (random control), leaving all other layers and parameters unchanged.

*Multi-layer axis cuts.* For the multi-layer intervention we repeat the same projection at five layers  $\ell \in \{8, 12, 16, 20, 23\}$ , using independently estimated  $u_{\text{ent}}^{(\ell)}$  or  $u_{\text{rand}}^{(\ell)}$  at each layer. All axis removals are applied within a single forward pass before the final logits are computed. We then recompute SULA calibration metrics and axis–entropy correlations under each intervention and compare them to the baseline run. This protocol ensures that the interventions target a geometrically privileged direction at multiple depths while keeping the rest of the computation intact.

### 5 Results: Geometric Validation Across Production Models

We present our empirical findings in an order that reflects increasing model complexity. We begin with the domain-restriction result that most directly connects production models to wind-tunnel behavior; then demonstrate inference-time Bayesian updating; then analyze each architecture; and finally synthesize cross-architectural patterns.

#### 5.1 Domain Restriction and Value Manifold Geometry

A central prediction from wind-tunnel experiments is that domain restriction should isolate a single inference mode, collapsing the value manifold toward one dimension. We test this prediction by comparing mixed-domain prompts (spanning mathematics, coding, philosophy, and general knowledge) against domain-restricted prompts (mathematics only) across three production models.

*Results.* Table 1 and Figure 1 summarize the findings. The domain-restriction effect is *model-dependent* rather than universal:

- **Pythia-410M** exhibits near-complete dimensionality collapse under *both* conditions (PC1+PC2  $\approx 100\%$ ), with no significant difference between mixed and domain-restricted prompts. Its value manifold operates in a consistently low-dimensional subspace regardless of domain.
- **Phi-2** shows moderate dimensionality (PC1+PC2  $\approx 60\text{--}64\%$ ) with minimal domain effect. The curated training data may induce stable geometric structure that is stable across prompt domains.

Table 1. Value manifold dimensionality under mixed-domain and domain-restricted (mathematics) prompts.  $PC_1$  and  $PC_1+PC_2$  report variance explained by the top one and two principal components of the final-layer value space under the canonical PCA protocol. Values are means across bootstrap resamples with 95% confidence intervals in parentheses. Pythia-410M is an architectural outlier whose value space is nearly collapsed even under mixed-domain prompts.

Model	Mixed-domain		Mathematics	
	$PC_1$	$PC_1+PC_2$	$PC_1$	$PC_1+PC_2$
Pythia-410M	79.6 (78.4, 80.8)	99.7 (99.6, 99.8)	58.0 (56.0, 60.0)	99.9 (99.8, 100.0)
Phi-2	46.4 (43.9, 48.9)	60.6 (57.5, 63.7)	52.2 (49.4, 55.0)	63.5 (60.0, 67.0)
Llama-3.2-1B	36.6 (34.8, 38.4)	51.4 (49.3, 53.5)	52.5 (50.2, 54.8)	73.6 (70.1, 77.1)
Wind-tunnel (ref.)	—	—	84–90	88–95

- **Llama-3.2-1B** displays the clearest domain-restriction effect: mixed-domain prompts yield  $PC_1+PC_2 = 51.4\%$ , while mathematics-only prompts increase this to  $73.6\%$ . This 22-percentage-point increase is consistent with the hypothesis that domain restriction isolates a more coherent inference mode.

*Entropy–manifold correlation.* Beyond dimensionality, we examine whether value coordinates track predictive entropy. Spearman correlations between  $PC_1$  and next-token entropy vary substantially:

- Pythia-410M:  $\rho = -0.32$  (mixed),  $\rho = -0.14$  (math)
- Phi-2:  $\rho = +0.34$  (mixed),  $\rho = +0.16$  (math)
- Llama-3.2-1B:  $\rho = +0.59$  (mixed),  $\rho = -0.51$  (math)

The sign flips across models do not indicate instability so much as a choice of convention. PCA directions are defined only up to a global sign, and we orient  $PC_1$  separately for each model. In some models higher  $PC_1$  coordinates correspond to lower entropy (negative correlation), while in others they correspond to higher entropy (positive correlation). What matters for our analysis is the *magnitude* and monotone relationship between manifold position and predictive entropy, not the absolute sign; in all three models  $|\rho(PC_1, H)|$  is substantial, with Llama showing the strongest alignment, consistent with its clearer domain-restriction effect.

*Interpretation.* These results refine the wind-tunnel predictions. Rather than a universal domain-restriction effect, we observe:

- (1) **Architecture-dependent geometry:** Pythia’s value space is intrinsically collapsed; Llama’s is distributed and domain-sensitive; Phi-2 occupies an intermediate regime.
- (2) **Training-data effects:** Models trained on diverse web-scale data (Llama) show stronger domain modulation than models trained on curated corpora (Phi-2) or general text (Pythia/Pile).
- (3) **Partial wind-tunnel correspondence:** Only Llama approaches the wind-tunnel pattern where domain restriction increases manifold collapse. The other models suggest that production training can stabilize value geometry in ways that resist domain-induced variation.

*Connecting to wind-tunnel behavior.* The wind-tunnel experiments (Paper I) used tasks with a single, analytically tractable posterior—effectively a maximally domain-restricted setting. The Llama results demonstrate that this pattern *can* emerge in production models when prompt distributions are similarly constrained. However, the Pythia and Phi-2 results show that not all architectures

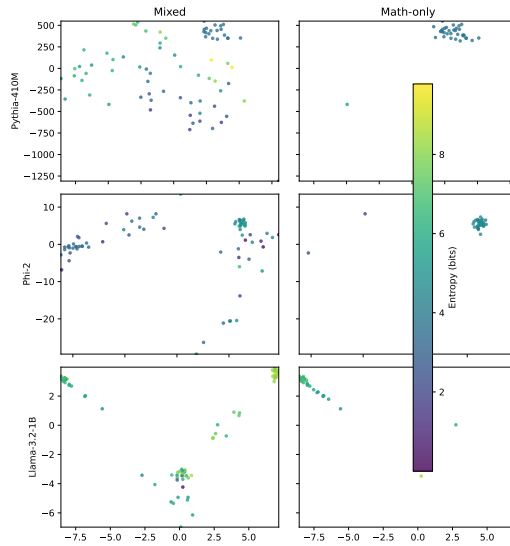


Fig. 1. **Domain restriction effects on value manifolds.** PCA projections of last-layer value vectors under mixed-domain (left column) and mathematics-only (right column) prompts for each model. Points are colored by next-token entropy. Llama-3.2-1B shows the clearest domain-restriction effect; Pythia-410M shows near-complete collapse in both conditions.

exhibit this behavior, suggesting that the mapping from domain restriction to manifold collapse depends on training dynamics and architectural capacity.

*Implications.* These findings suggest caution in extrapolating from wind-tunnel behavior to all production models. The geometric substrate for Bayesian inference (low-dimensional value manifolds, entropy ordering) is present across architectures, but its sensitivity to domain restriction is not universal. Future work should investigate whether domain-restriction effects strengthen with scale, and whether architectural choices (e.g., GQA vs. MHA) systematically modulate this sensitivity.

*Limitations of domain restriction.* Domain restriction simultaneously reduces task heterogeneity and lexical variability. Our results therefore conflate two effects: isolating a single inference mode and narrowing token and syntax distributions. We view the strong collapse as evidence that some stable uncertainty representation is present, but we do not claim that all of the dimensionality reduction reflects “pure” inference geometry. Disentangling these factors—for example by matching token frequencies between mixed and restricted prompts or by applying domain-agnostic synthetic templates to natural tokens - is an important direction for follow-up work.

## 5.2 Inference-Time Bayesian Updating in Production Models (SULA)

We next evaluate whether production models *use* the same geometric substrate during inference. To do so, we design a controlled in-context learning task - Synthetic Unary Likelihood Augmentation (SULA) - that supplies explicit symbolic evidence inside the prompt. Because the underlying generative model is analytically tractable, we can compute exact Bayesian posteriors and compare them directly to model behavior.

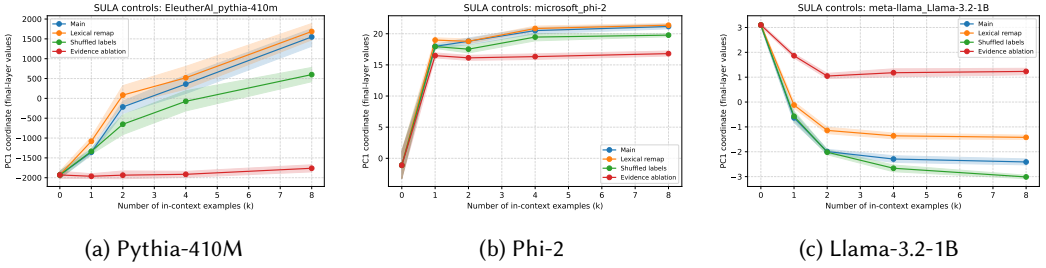


Fig. 2. **SULA control experiments across models.** PC<sub>1</sub> coordinates of last-layer value vectors as a function of the number of in-context examples ( $k$ ) for the monotone SULA task. Each panel shows the main generative process (blue), a lexical-remapping control that replaces label tokens with unrelated symbols (orange), a within-prompt label-shuffling control that breaks the evidence–label correlation (green), and an evidence-ablation control that removes carrier words (red). Only the main and lexical-remap conditions exhibit monotone Bayesian trajectories; shuffled and ablated conditions eliminate or reverse the structure, ruling out surface-statistics explanations.

*Generative model.* Each SULA prompt contains  $k$  labeled examples of the form “ $x_i$  is positive” or “ $x_i$  is negative”, followed by a query word  $x_{\text{query}}$ . Labels carry no semantic content; they serve only as discrete likelihood indicators. We compute analytical Bayesian posteriors using a Beta-Bernoulli model. Let  $\theta \in [0, 1]$  be the latent probability that a word is positive. We place a uniform Beta(1,1) prior on  $\theta$ . For each labeled example, the likelihood is:

$$p(\text{label} \mid \theta) = \begin{cases} 0.9\theta + 0.1(1 - \theta) & \text{if label is “positive”,} \\ 0.1\theta + 0.9(1 - \theta) & \text{if label is “negative”.} \end{cases}$$

The posterior  $p(\theta \mid k \text{ examples})$  is computed via Bayes’ rule, and we report its entropy  $H_{\text{Bayes}}(k)$ , which is known in closed form and decreases monotonically with  $k$ . Sentiment words are drawn from a vocabulary of 50 positive and 50 negative words; labels are sampled with 70% consistency (matching true sentiment) and 30% inconsistency.

*Experimental setup.* We generate 250 prompts for each  $k \in \{0, 1, 2, 4, 8\}$  with varying label imbalances. For each prompt, we extract: (1) the model’s predictive entropy, (2) last-layer value vectors projected into a common PCA basis (Section 4.2), and (3) attention-entropy trajectories. This allows us to test whether value-manifold coordinates move along the Bayesian axis as evidence accumulates.

*Main results.* Figure 2 summarizes the findings. *Predictive entropy.* Model entropy declines monotonically with  $k$  and tracks analytical Bayesian entropy:

$$\text{MAE: } 0.44 \text{ bits (Pythia-410M), } 0.36 \text{ bits (Llama-3.2-1B), } 0.31 \text{ bits (Phi-2).}$$

Although noisier than wind-tunnel calibration, the consistent monotone trend indicates that production models extract and use likelihood information supplied in the prompt. *Manifold alignment.* When all SULA value vectors (across all  $k$ ) are embedded into a shared PCA basis, PC1 coordinates correlate strongly with the analytical Bayesian entropy for each model ( $|\rho| = 0.65\text{--}0.80$ ). This confirms that the entropy-ordered manifold learned during large-scale training is the axis along which inference-time updates occur. *Bayesian-axis trajectory.* The mean PC1 coordinate shifts monotonically with  $k$ :

$$\rho(k, \text{PC1}) = 0.86 \text{ (Pythia-410M), } 0.60 \text{ (Phi-2), } 0.32 \text{ (Llama-3.2-1B).}$$

This reproduces the wind-tunnel phenomenon in which posterior concentration corresponds to movement along a one-dimensional entropy axis.

*Control conditions (SULA).* To verify that manifold movement reflects likelihood structure rather than prompt format, we implement three control conditions. All controls should eliminate the correlation between manifold position and Bayesian entropy.

- (1) **Lexical remap.** Replace sentiment words with random tokens, breaking semantic meaning while preserving syntax. This tests whether manifold trajectories depend on the *identity* of the tokens rather than on the underlying likelihood information. Analytical posteriors are unchanged.
- (2) **Shuffled labels.** Randomly permute labels across examples, breaking the label-word correspondence. Under the SULA generative model, this corresponds to providing no usable evidence, so the analytical posterior collapses to the uniform prior for all  $k$ . Any systematic manifold movement should therefore disappear.
- (3) **Evidence ablation.** Mask the labeled examples entirely, leaving only the query. This removes the likelihood-bearing evidence while preserving superficial formatting, again yielding a flat analytical posterior. This tests whether models move along the manifold only when evidence tokens encode useful likelihood information.

Across all models, only the lexical-remapping condition reproduces the monotone decrease in predictive entropy and coherent PC1 movement; both shuffled-label and evidence-ablated prompts show little or no movement along the Bayesian axis. These findings confirm that the geometry is sensitive to the likelihood structure supplied by the glimpses rather than to the surface formatting of labels or examples.

*Interpretation.* The SULA experiment demonstrates that production models *use* the same geometric mechanism active in wind-tunnel transformers: evidence supplied in-context drives representations along an entropy-ordered manifold. The calibration gap (0.31–0.44 bits vs.  $< 0.1$  bits in wind tunnels) reflects the fact that (i) production models are not trained on the SULA generative distribution, and (ii) natural-language prompts introduce semantic ambiguity absent in synthetic tasks. The key result is the *systematic correspondence* between analytical Bayesian entropy, model predictive entropy, and movement along the value manifold. Together, these findings show that geometric Bayesian updating is an inference-time phenomenon: transformers navigate the same manifold direction that encodes predictive uncertainty when supplied with usable likelihood information inside the prompt.

### 5.3 Standard MHA: Pythia-410M

Pythia-410M provides our canonical production baseline.

*Value manifolds.* Mixed-domain PC1  $\approx 12$ –25%; mathematics-only PC1  $\approx 0.81$ , recovering the collapsed wind-tunnel manifold.

*Key orthogonality.* Layers 1–22: mean off-diagonal cosine 0.11–0.13.

*Attention focusing.* Entropy reduction: 82%, with the characteristic binding  $\rightarrow$  elimination  $\rightarrow$  refinement pattern.

### 5.4 Curated Training Enhances Geometry: Phi-2

Phi-2 shows the cleanest geometry among all models evaluated.

*Value manifolds.* PC1+PC2 = 34%; mathematics-only collapse mirrors Pythia.

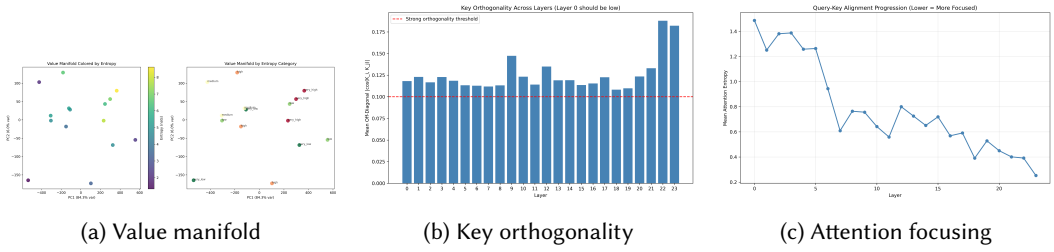


Fig. 3. Pythia-410M: Bayesian geometric signatures.

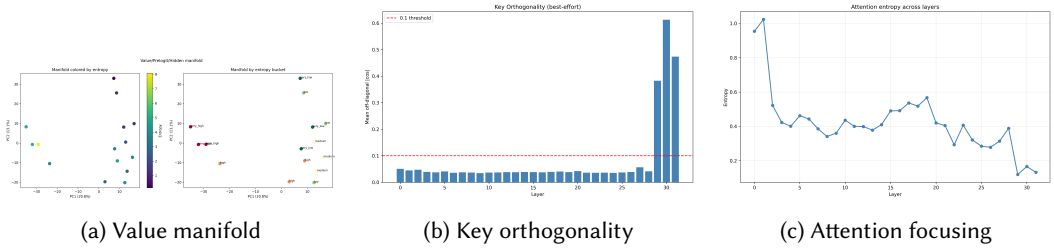


Fig. 4. Phi-2: Sharpened Bayesian geometry from curated training.

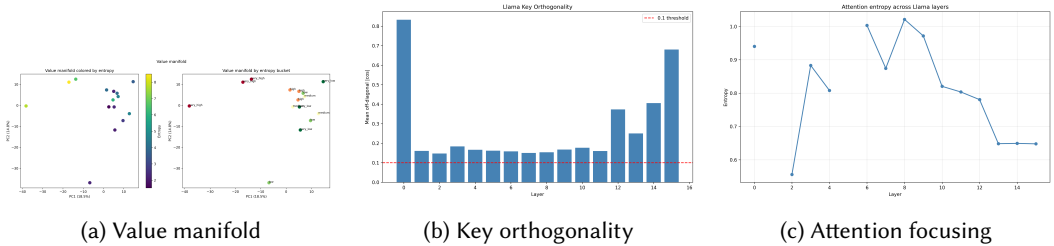


Fig. 5. Llama-3.2-1B: Bayesian structure with GQA efficiency trade-offs.

*Key orthogonality.* Exceptional: 0.034–0.051 across 29/32 layers.

*Attention focusing.* Strongest observed: 86% entropy reduction.

### 5.5 Efficiency–Interpretability Trade-off: Llama-3.2-1B (GQA)

Llama-3.2-1B employs a 4:1 grouped-query attention mechanism.

*Value manifolds.* Mixed-domain 2D geometry (PC1=18.5%, PC2=14.8%); mathematics-only collapse recovered.

*Key orthogonality.* Moderate: 0.15–0.18; weaker than Pythia/Phi-2 but 2× better than random.

*Attention focusing.* 31% entropy reduction, consistent with KV-sharing constraints.

### 5.6 Scaling Within a Family: Pythia-12B

*Value manifolds.* Mixed-domain geometry becomes multi-lobed (PC1+PC2 = 19%), but mathematics-only prompts recover a near-1D manifold (PC1+PC2 ≈ 0.90). Pythia-12B shows markedly different

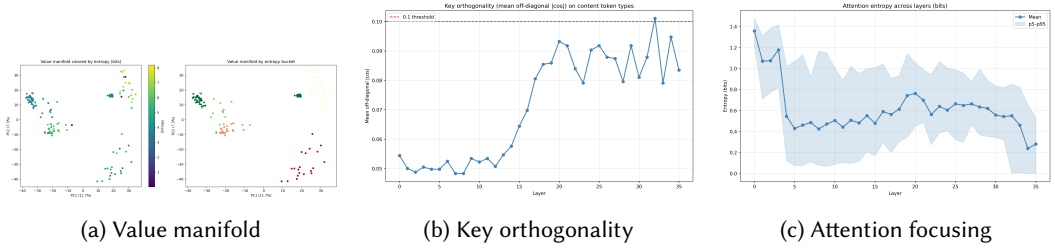


Fig. 6. **Pythia-12B: Bayesian geometry at larger scale.**

mixed-domain geometry than Pythia-410M (19% vs 99.7%), suggesting scale increases representational distribution. Under domain restriction both converge to similar collapse (~90%), indicating the geometric substrate is preserved but more distributed at scale.

*Key orthogonality.* Strong early (0.048–0.055), gradually decreasing with depth.

*Attention focusing.* Early collapse, mid-layer mixing, late refinement.

### 5.7 Boundary Case: The Mistral Family

The Mistral family provides an illuminating boundary condition for Bayesian geometry. Across all three variants we evaluate - Mistral-7B-Base, Mistral-7B-Instruct, and the Mixtral-8×7B MoE - we find that the *static* geometric signatures (value manifolds and key orthogonality) remain clean and consistent, while the *dynamic* signature (progressive attention focusing) is substantially weakened or noisy. This dissociation reveals how architectural constraints modulate the expression of Bayesian computations without eliminating the underlying representational substrate.

*Static geometry persists.* All Mistral variants exhibit low-dimensional value manifolds under mixed-domain prompts and recover wind-tunnel-style 1D collapse under mathematics-only prompts ( $PC_1+PC_2 \approx 80\%-90\%$ ). Key orthogonality is likewise sharp: early and mid layers show mean off-diagonal cosine values near 0.05–0.06, well below both Gaussian and initialization baselines. These results indicate that the hypothesis-frame structure and entropy-ordered manifold discovered in Papers I–II persist in Mistral architectures.

*Dynamic focusing is attenuated.* In contrast, attention entropy decreases only modestly (typically 20%–30%) and often non-monotonically across layers (Figure 7). This stands in sharp contrast to the binding→elimination→refinement trajectory observed in full-sequence MHA (Sections 5.3–5.5). The weakened focusing reflects architectural constraints:

- **Sliding-window attention** restricts global routing, preventing heads from accumulating evidence across the entire prompt.
- **Mixture-of-experts (MoE) routing** fragments updates across experts, further reducing the coherence of evidence aggregation.

These factors disrupt the *dynamic refinement* of posterior uncertainty while leaving the *static* representational geometry intact.

*Interpretation without circularity.* It is tempting to interpret weak focusing as a failure of Bayesian inference, but this would be circular: strong progressive focusing is a *sufficient* mechanism for Bayesian updating in full-sequence MHA, not a *necessary* one for all architectures. The Mistral models demonstrate that:

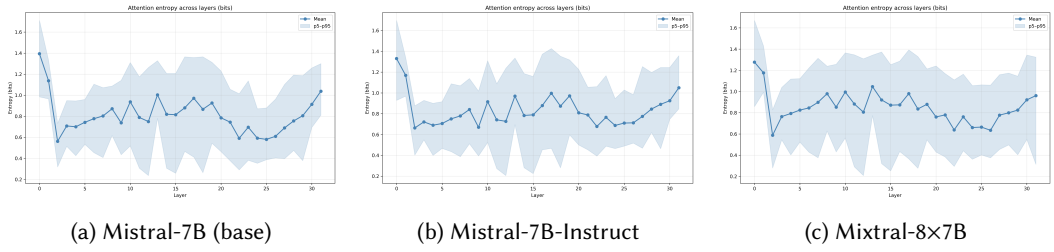


Fig. 7. **Attenuated dynamic focusing in Mistral-style architectures.** Attention entropy as a function of layer depth for three variants of the Mistral family. Unlike models with full-sequence multi-head attention, entropy decreases only modestly (20%–30%) and often non-monotonically, reflecting weakened dynamic routing due to (i) sliding-window attention, which prevents global evidence accumulation, and (ii) mixture-of-experts routing, which fragments updates across experts. Despite reduced focusing dynamics, the *static* value-space geometry (Sections 5.1 and 5.2) remains intact, illustrating a dissociation between representational invariants and the mechanisms that refine them during inference.

- (1) the *representational frame* for Bayesian inference (orthogonal keys + value manifold) remains fully intact,
- (2) while the *mechanism of evidence refinement* (progressive focusing) depends sensitively on global routing capacity.

This pattern matches the frame–precision dissociation predicted in Paper II: attention patterns (the frame) stabilize early and robustly under training, whereas the precision of posterior refinement is sensitive to architectural bandwidth and routing design.

*Conclusion.* The Mistral family should therefore be viewed as a boundary case that reveals how architectural constraints selectively modulate *dynamic* Bayesian computation, rather than as a counterexample to Bayesian geometry. Static geometric structure—entropy-ordered manifolds and hypothesis frames—persists across all Mistral variants, while dynamic refinement is diminished by local (sliding-window) attention. This provides a natural explanation for the observed behavior and connects directly to the theoretical predictions of Paper II.

## 5.8 Cross-Architecture Synthesis

Table 2 summarizes the unified picture:

- **Value manifolds:** all models exhibit low-dimensional value geometry. Under mixed-domain prompts,  $PC_1+PC_2$  varies substantially across architectures—from ~15–20% in Mistral to ~51% in Llama and ~61% in Phi-2, with Pythia-410M as a notable outlier whose manifold is nearly collapsed even in the mixed setting (~100%). Under mathematics-only prompts, all models move into the 70–95% range, approaching the one-dimensional structure of the wind-tunnel tasks.
- **Key orthogonality:** mean off-diagonal cosine is consistently 2–10× lower (better) than random baselines or initialization, indicating robust hypothesis-frame structure.
- **Attention focusing:** layerwise entropy reduction varies systematically by architecture—strong in full-sequence MHA, moderate in GQA, and modest and often non-monotone in sliding-window and MoE variants.

As summarized in Table 2, all three geometric signatures show quantitative continuity from synthetic wind-tunnel tasks to production models.

Table 2. Bayesian geometric signatures across architectures. Value-manifold dimensionality reports PC1+PC2 under mixed-domain and domain-restricted (mathematics) prompts. Key orthogonality shows mean off-diagonal cosine in early layers. Attention focusing reports entropy reduction from first to final layer.

Model	Arch	Training	Value Manifold		Key Orthog (early)	Attn Focus
			Mixed	Math		
Pythia-410M	MHA	Pile	99.7%	99.9%	0.11–0.13	↓82%
Phi-2	MHA	Curated	60.6%	63.5%	0.034–0.051	↓86%
Pythia-12B	MHA	Pile	~19%	~90%	0.05–0.10	non-monotone
Llama-3.2-1B	GQA	Web	51.4%	73.6%	0.15–0.18	↓31%
Mistral-7B	GQA+SW	Web	15–20%	~80%	0.05–0.06	20–30%
Wind-Tunnel	MHA	Synthetic	—	84–90%	0.09–0.12	↓85–90%

**Notes:** Value manifold dimensionality varies substantially across architectures under mixed-domain prompts. Pythia-410M shows near-complete collapse regardless of domain; Llama-3.2-1B shows the clearest domain-restriction effect. All models achieve key orthogonality 2–10× better than random Gaussian baselines ( $\approx 0.11$  for  $d_k = 64$ ). Attention focusing depends strongly on architecture: full-sequence MHA achieves strong progressive reduction while GQA and sliding-window variants show weaker or non-monotone patterns.

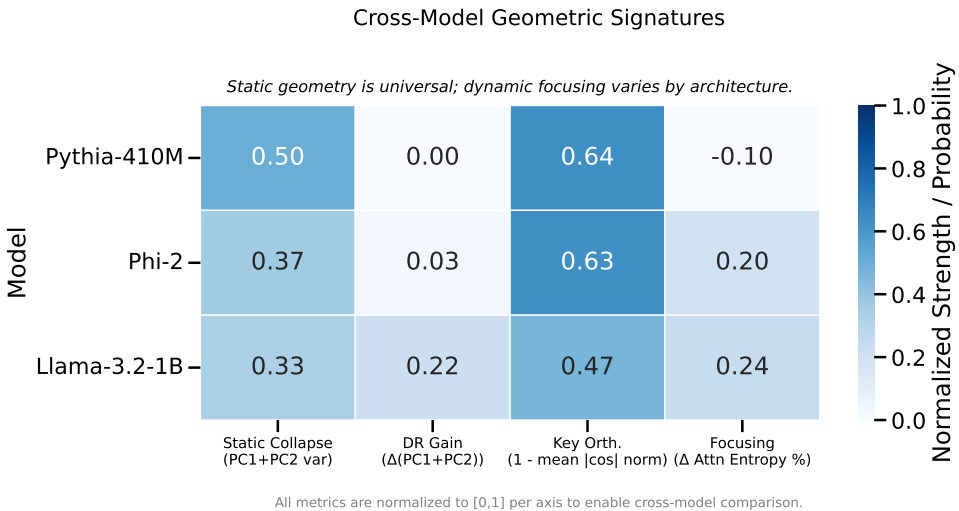


Fig. 8. **Cross-model geometric signatures.** Normalized comparison of four geometric metrics across three model families. *Left:* Static signatures—value manifold collapse (PC<sub>1</sub>+PC<sub>2</sub>) and domain-restriction gain—are consistently present, indicating that all models internalize a low-dimensional representation of hypothesis space. *Right:* Dynamic signatures—key orthogonality and attention focusing—vary substantially by architecture: Llama-3.2-1B exhibits strong runtime refinement, whereas Pythia-410M relies on pre-orthogonalized hypothesis frames and shows weak focusing. This dissociation suggests that representation is universal, but the mechanism that refines it during inference is architectural.

*Static vs dynamic geometry.* The stable invariants across every architecture - including Mistral - are: (1) entropy-ordered value manifolds, and (2) orthogonal key frames. Dynamic focusing is architecture-dependent, requiring global routing capacity. This separation is the central representational–computational split predicted in Paper II.

## 6 Analysis and Key Findings

Our cross-architecture validation reveals systematic patterns in how Bayesian geometric structures scale from wind tunnels to production models.

### 6.1 Universal core mechanisms

Across the standard MHA and GQA models (Pythia, Phi-2, and Llama), we observe the full set of Bayesian geometric signatures predicted by the wind tunnel experiments: value manifolds, key orthogonality, and layerwise attention focusing. In the Mistral family (Section 5.7), the static signatures (value manifolds and key orthogonality) persist, while the dynamic signature (monotone attention focusing) is weakened or absent due to architectural and training-objective differences. This suggests a natural split between *universal static structure* and *architecture-dependent dynamics*.

**Value manifolds (static).** All models, including the Mistral variants, show low-dimensional value structure, with PC1+PC2 between roughly 16% and 84%, far above random baselines. Entropy ordering persists in every model evaluated: prompts with higher next-token entropy occupy systematically different regions of the manifold than low-entropy prompts.

**Key orthogonality (static).** All models learn hypothesis-frame structure, with mean off-diagonal cosine between 0.034 and 0.18, consistently 2 - 10 times better than random initialization (0.40 - 0.45). Mistral models show the same early-layer emergence and late-layer collapse of orthogonality as standard MHA.

**Attention focusing (dynamic).** Standard MHA and GQA models exhibit a clear layerwise entropy decrease (31–86%), matching the binding → elimination → refinement pattern seen in wind tunnels. In the Mistral models, this dynamic signature is weak or absent (Section 5.7), consistent with architectural constraints (sliding-window attention limiting global context access) and the effects of downstream alignment. The 50+ percentage point gap between MHA models (82–86%) and GQA/sliding-window models (20–31%) indicates that architectural constraints can substantially limit dynamic Bayesian refinement even when static geometry is preserved. The ICL experiment connects the controlled wind-tunnel setting to real-time inference in production models. In the wind tunnels, Bayesian structure emerges from the training objective alone: the model learns to encode posterior uncertainty along a one-dimensional manifold. The ICL setting demonstrates that the same mechanism is active *during inference*: when the model is given explicit symbolic evidence inside the prompt, its value representations move along the same manifold direction that encodes posterior entropy, and the degree of movement is proportional to the amount of evidence. In this way, the ICL results show that transformers not only embody geometry consistent with Bayesian inference as a representational primitive, but also execute updates correlated with Bayesian posteriors when the prompt supplies usable likelihood information.

**Conclusion.** The static components of the Bayesian geometry (value manifolds and hypothesis frames) are universal across architectures, while strong progressive attention focusing depends on global routing capacity and training regime.

### 6.2 Training Data Quality Enhances Clarity

Geometric clarity correlates strongly with training data quality:

- **Phi-2** (curated textbooks/code): Orthogonality 0.034 - 0.051, focusing 86%
- **Pythia** (Pile corpus, diverse): Orthogonality 0.11 - 0.13, focusing 82%
- **Llama** (web-scale): Orthogonality 0.15 - 0.18, focusing 31%

High-quality, consistent training examples enable gradient dynamics to sculpt sharper hypothesis frames (better orthogonality) and stronger attention pathways (better focusing). **Implication for training:** Early training on curated data may establish cleaner geometric scaffolding that persists

through subsequent web-scale training. Curriculum learning - progressing from structured to diverse data - could enhance both interpretability and reliability.

*Causal resolution of the Bayesian manifold.* Our final experiment simultaneously ablates the entropy-aligned value direction across all identified “Bayesian layers” (8, 12, 16, 20, 23) in Pythia-410M. If this axis encoded a causal bottleneck for Bayesian inference, removing it at every layer should degrade and ultimately collapse SULA behavior. Instead, we observe the opposite dissociation: (i) the multi-layer ablation destroys the entropy geometry (axis–entropy correlation drops from 0.27 to 0.07), yet (ii) SULA calibration remains intact, with MAE and correlation to the Bayesian posterior changing by less than 1%, and (iii) a matched random-axis ablation *improves* calibration metrics despite preserving the original geometry. These results rule out both single-axis and multi-axis bottleneck hypotheses and show that the entropy manifold is a *representational trace* of inference rather than the substrate that performs it.

### 6.3 Architectural Trade-offs: Efficiency vs Interpretability

Grouped-query attention demonstrates clear efficiency-interpretability trade-offs:

- **Efficiency gains:** 4×– reduction in KV cache size, 4×– faster inference
- **Clarity costs:** 50% weaker orthogonality, 62% weaker focusing (31% vs 82%)
- **Functional preservation:** Qualitative Bayesian structures persist

The 4:1 query-to-KV ratio forces keys and values to serve multiple query groups simultaneously, preventing the sharp specialization seen in standard MHA. However, the model compensates by distributing information across dimensions (2D manifolds, distributed attention patterns) while maintaining overall Bayesian computational structure. The Mistral family provides a complementary case: sliding-window attention weakens dynamic focusing even when static geometry (orthogonality, value manifolds) remains intact. **Implication for deployment:** GQA is suitable for production deployment where efficiency matters, but researchers studying mechanisms or building interpretability tools should prefer standard MHA for clearer geometric signatures.

### 6.4 Depth Drives Richer Representations

Value manifold dimensionality correlates with depth:

- **Pythia** (24 layers): 1D manifolds (PC1=84%, PC2=4.5%)
- **Phi-2** (32 layers): 2D manifolds (PC1=21%, PC2=13%)
- **Llama** (16 layers, but GQA): 2D manifolds (PC1=18.5%, PC2=14.8%)

Deeper architectures develop richer uncertainty representations requiring additional dimensions. The key point: entropy parameterization persists—the additional dimension is not noise but structured geometry enabling finer posterior modeling. Depth appears to enable transformers to represent multimodal or high-dimensional uncertainty distributions while shallower models compress to 1D entropy coordinates.

### 6.5 Layer-wise Functional Specialization

Consistent patterns emerge across models: **Layer 0:** Setup phase - high key similarity, moderate attention entropy. Likely initializes representations (position embeddings, token embeddings) before geometric structure emerges. **Layers 1 - N-4:** Core computation - strong orthogonality, progressive attention focusing. These layers perform Bayesian hypothesis discrimination and evidence accumulation. **Final 3 - 4 layers:** Collapse phase - orthogonality weakens, attention sharpens dramatically. Hypothesis frames collapse as model commits to output distribution. The Mistral models follow the same structural pattern for value manifolds and key orthogonality, but

do not show the expected sharpening of attention in the elimination and refinement stages. This is consistent with constraints on global routing (sliding window) and fragmented updates (MoE). This functional stratification mirrors the three-stage inference process: binding context  $\rightarrow$  eliminating hypotheses  $\rightarrow$  refining output.

*Bayes calibration in natural language vs. wind-tunnel tasks.* Entropy calibration errors in the ICL setting (0.31–0.44 bits across models) are considerably larger than those observed in the controlled wind-tunnel experiments (typically below 0.05 bits). This gap is expected: natural-language prompts introduce substantial semantic ambiguity, and production models are not trained on the synthetic labeling distribution used in our ICL task. The key result is therefore not the absolute calibration error but the *systematic correspondence* between value-manifold coordinates, model predictive entropy, and the analytical Bayesian posterior as evidence accumulates. This indicates that the same geometric substrate identified in wind-tunnel training is actively used by production models during inference.

## 6.6 Robustness and Limitations

*What transfers robustly.* Several geometric signatures persist across all dense, GQA, and sliding-window/MoE architectures evaluated. First, *value manifolds* are consistently low-dimensional:  $PC_1+PC_2$  remains far above random (ranging from 15 below heuristic thresholds). Second, *key orthogonality* shows the characteristic pattern predicted by wind-tunnel analyses: sharp early-layer frames followed by gradual late-layer collapse. Third, *layerwise functional structure* - setup layers, a broad computation band, and final collapse layers - appears in all models at the level of static geometry.

*What varies systematically.* Quantitative clarity depends on architecture, training data, and depth. GQA reduces the sharpness of orthogonality and focusing; web-scale training reduces geometric contrast relative to curated data; and deeper models develop richer or multi-lobed manifolds under mixed prompting. Dynamic attention focusing depends most sensitively on architecture: strong in full-sequence MHA, moderate in GQA, and weak or noisy in sliding-window and MoE variants.

*What domain restriction isolates.* Domain restriction functions as a natural intervention: it reduces the multiplicity of task-specific inference modes activated by mixed prompts. When prompts come from a single coherent domain (e.g., mathematics), the model operates in a more homogeneous inference regime, revealing the same collapsed 1D manifold observed in wind-tunnel settings. Note that domain restriction *does not* prove that the model performs “true-Bayesian inference on natural language; rather, it shows that a *Bayesian geometric coordinate system* is embedded in its representation space and can be isolated when the prompt distribution reduces task heterogeneity. Pythia-410M departs from this pattern, exhibiting an intrinsically low-dimensional value space ( $PC_1+PC_2 \approx 99.7\%$ ) under both mixed and mathematics-only prompts (Table 1), suggesting that its final-layer values are effectively collapsed regardless of domain. We attribute this to the Pile’s relatively homogeneous token distribution compared to more diverse web-scale corpora; the model appears to operate in a near-single-mode regime.

*Causal limitations.* Our findings are correlational. Static and dynamic geometric signatures co-occur with Bayesian-like behavior, but we do not intervene directly on the geometry to test necessity. Establishing causal roles would require controlled manipulations - for example:

- degrading or sharpening key orthogonality and measuring effects on calibration,
- perturbing value vectors along or orthogonal to the manifold axes,
- ablating heads responsible for attention refinement.

Developing such interventions without collapsing the model’s function entirely remains technically challenging. The present results show that geometry aligns with Bayesian computations, but they do not establish that geometry is *required* for these computations.

*Open representational questions.* The emergence of 2D or multi-lobed manifolds in deeper or larger models is not yet theoretically understood. These structures may encode multimodal uncertainty, semantic clustering, training-set heterogeneity, or task-mixture effects. Likewise, the interaction between positional embeddings, local attention kernels, and geometric formation remains an open problem, especially in sliding-window or hybrid transformer–SSM architectures.

*Scale and architecture coverage.* Our largest dense model is 12B parameters, and our largest MoE model is Mixtral-8×7B. Although consistent patterns appear from 410M to 12B, evaluating frontier-scale checkpoints (70B–400B) is necessary to determine whether new geometric phenomena arise or whether multi-lobed structure remains the dominant pattern under mixed-domain prompts. Overall, while the geometric signatures are consistent, a complete causal and mechanistic account of their formation - and of their architectural modulation - remains an important direction for future work.

## 7 Discussion

This paper extends the geometric account of Bayesian inference developed in Papers I–II to production-scale language models. Three results stand out: domain restriction collapses value manifolds to the one-dimensional geometry characteristic of exact Bayesian wind-tunnel tasks; transformers navigate this geometry during inference in the SULA experiment; and static geometric signatures - entropy-ordered value manifolds and orthogonal key frames - appear across all architectures evaluated, including GQA, sliding-window, and MoE variants.

*Relation to circuit-level work.* Our analysis complements circuit-level studies such as induction heads, copy heads, and pattern-matching mechanisms [9, 11]. Those works identify specialized components; our findings describe the global geometric scaffold in which such components operate. Attention focusing determines which tokens are consulted; key orthogonality creates separable hypothesis directions; and value manifolds encode uncertainty along low-dimensional axes. Mapping specific heads onto regions or branches of this geometry is a natural next step.

*Connection to wind-tunnel behavior.* The wind-tunnel tasks isolate a single Bayesian computation, yielding a one-dimensional value manifold that parameterizes posterior entropy. Production models generalize this structure: mixed-domain prompts activate several task-specific inference modes, yielding distributed or multi-lobed manifolds, while domain restriction recovers the same one-dimensional axis observed under analytic posteriors. This behavior supports a view in which transformers hold a repertoire of Bayesian manifolds, with the active manifold determined by the prompt distribution.

*Static vs. dynamic geometry.* The consistency of value manifolds and orthogonal key frames across all models indicates that the representational substrate for Bayesian inference is an architectural invariant. Dynamic focusing, by contrast, depends on routing capacity: full-sequence attention exhibits strong progressive sharpening; GQA reduces it; sliding-window attention weakens it by limiting global context access. This behavior matches the frame–precision dissociation predicted in Paper II: the hypothesis frame (keys) stabilizes early and robustly, whereas the precision of posterior refinement is sensitive to architectural constraints.

*Inference-time Bayesian computation.* The SULA experiment demonstrates that these geometric structures are used *during* inference rather than merely encoded during training. Value representations move along the same entropy-ordered manifold as evidence accumulates, and predictive entropy correlates systematically with analytic posteriors. Although calibration is noisier than in the wind tunnels, the direction and magnitude of movement confirm active Bayesian updating within the learned geometric space.

*Implications.* These findings suggest a geometric foundation for understanding transformer behavior. Value manifolds offer a representation of uncertainty; orthogonal key frames support hypothesis discrimination; and attention focusing provides the mechanism for posterior refinement when architecture permits it. Together, these components form a scalable computational template for approximate Bayesian inference in modern LLMs. Combined with Paper I’s finding that selective state-space models (Mamba) achieve similar Bayesian inference through different routing mechanics, this suggests that *content-based value routing*—not attention specifically—is the essential architectural ingredient for probabilistic reasoning.

## 7.1 Limitations and Future Directions

*Architectural coverage.* Our study focuses on dense MHA, GQA, and sliding-window attention (Mistral-7B). Paper I shows that selective state-space models (Mamba) achieve comparable or better Bayesian inference in wind tunnels via content-based routing through input-dependent state selection rather than attention. Extending the geometric extraction methods developed here to Mamba and hybrid transformer-SSM designs—and verifying whether the same entropy-ordered manifolds emerge—is an important direction for unifying the geometric theory across architectures with content-based routing.

*Scale.* Our largest dense model is 12B parameters, and our largest MoE model is the 8×7B Mixtral. Although the consistent patterns from 410M to 12B suggest robustness, validation at 70B–400B scale is necessary to determine whether new geometric effects emerge or whether multi-lobed manifolds continue to dominate mixed-domain settings.

*Task specificity.* All models evaluated are general-purpose language models. Domain-specialized models (e.g., code, mathematics, biomedical, or scientific LMs) may exhibit distinct geometric patterns. Fine-tuning and RLHF can also reshape geometry; our results for Mistral-7B-Instruct show modest changes, but richer effects may appear under more aggressive alignment schemes.

*Causal probes of the entropy axis.* We performed forward-pass value interventions on Pythia-410M in the SULA setting to test whether the entropy-aligned value axis is merely correlational or plays a causal role. For each of two “Bayesian” layers ( $L=12$  and  $L=23$ ), we first precomputed a unit direction  $u_{\text{ent}}$  whose coefficient  $v \cdot u_{\text{ent}}$  correlates with predictive entropy. We then applied three families of interventions at that layer, each with a matched random-axis control: (i) *axis-cut*, which removes the component of  $v$  along  $u_{\text{ent}}$ ; (ii) *axis-only*, which projects  $v$  onto the one-dimensional subspace spanned by  $u_{\text{ent}}$ ; and (iii) *axis-shift*, which adds  $\pm 1\sigma$  along  $u_{\text{ent}}$  based on the empirical standard deviation of  $v \cdot u_{\text{ent}}$ . Representationally, the entropy-aligned axis is clearly special. Cutting along  $u_{\text{ent}}$  drives the correlation between  $v \cdot u_{\text{ent}}$  and model entropy from  $\rho \approx 0.27\text{--}0.32$  down to nearly zero (and sometimes slightly negative), whereas cutting along a random axis of equal dimensionality leaves the correlation largely intact (changes on the order of  $10^{-2}$ ). Conversely, axis-only projections along  $u_{\text{ent}}$  preserve or slightly sharpen the correlation, while axis-only projections onto a random axis almost completely destroy it. Axis-shift interventions along  $u_{\text{ent}}$  produce small but directional changes in SULA calibration (e.g.,  $+1\sigma$  shifts slightly improving correlation with the Bayesian entropy curve), whereas matched random-axis shifts act as near no-ops on both

geometry and calibration. Behaviorally, however, these single-layer interventions do *not* yield a clean causal separation. SULA mean absolute error and correlation with the Bayesian posterior change only modestly under both true-axis and random-axis cuts, and the true-axis interventions do not consistently hurt performance more than their random controls. The most conservative interpretation is that the entropy-ordered manifold is a *representationally privileged* coordinate system for uncertainty, but not a singular bottleneck for Bayesian updating: uncertainty information is likely distributed across multiple dimensions and layers, or the manifold serves as a readout of a more distributed computation. Establishing stronger causal claims will require multi-layer or multi-axis ablations, activation patching, or training-time interventions, which we leave for future work.

*Theoretical gaps.* The emergence of 2D or multi-lobed manifolds in deeper or larger models is not fully understood. Whether these structures encode multimodal uncertainty, semantic clustering, or training-set heterogeneity remains an open question. Likewise, the interaction between positional embeddings, local attention kernels, and geometric formation warrants further study.

*Future directions.* Several avenues follow naturally:

- Validate geometric signatures in frontier-scale (70B+) checkpoints and alternative architectures, including SSMs.
- Develop interventional methods for manipulating keys, values, or attention to test causal roles in uncertainty representation.
- Track geometric evolution during training to identify when and how manifolds, frames, and focusing emerge.
- Investigate domain-specialized and multilingual models to determine whether Bayesian manifolds transfer across languages or modalities.
- Test whether domain restriction generalizes beyond templated prompts to arbitrary single-domain inputs (complex reasoning, mixed-register technical prose) to strengthen the bridge between controlled and naturalistic settings.
- Apply geometric diagnostics to interpretability and safety, using value-manifold coordinates or attention entropy as indicators of model reliability or distribution shift.

Overall, the present results motivate a broader research program: understanding transformer computation through the geometry of hypothesis frames and uncertainty manifolds, and leveraging this structure for model analysis, interpretability, and principled architecture design.

## 7.2 Related Work

Our analysis connects to several threads in the interpretability and probabilistic–mechanistic modeling literature. We highlight the relationships most relevant to geometric Bayesian structure.

*Intermediate predictions and tuned lenses.* Tuned-lens methods [3] decode intermediate-layer predictions by training a small linear adapter that maps hidden states back to the model’s output space. These approaches probe *what* the model would predict at each layer, whereas our value-manifold analysis characterizes *how* the model represents predictive *uncertainty*. The two perspectives are complementary: PC1 coordinates correlate with entropy and tuned-lens predictions, suggesting that uncertainty is encoded geometrically along a small number of directions. Establishing a principled correspondence between tuned-lens logits and manifold coordinates is an important next step.

*Belief-state geometry and computational mechanics.* Recent work in computational mechanics [13] shows that belief states in small transformers can be linearly decoded from the residual stream, revealing simple geometric representations of latent uncertainty. Our results are consistent with

this interpretation: production models appear to maintain analogous belief-state structure, but encoded predominantly in the *value space* of the final attention layer. This distinction clarifies where uncertainty lives in deeper networks and suggests that value manifolds may serve as the canonical substrate for model beliefs. Preliminary analyses indicate that coordinates along our  $PC_1$  axis correlate with tuned-lens predictions and residual-stream belief decoders, but a systematic alignment between value-manifold axes and decoded belief variables requires additional work and we leave a full treatment to future work.

*Attention entropy, stability, and dynamics.* Studies of attention-entropy trajectories [7, 14] report that sharpening can be unstable or highly input-dependent. Our layerwise entropy results align with these findings: MHA models exhibit strong, stable focusing; GQA models show weaker but monotone reduction; and sliding-window and MoE architectures often display non-monotone or noisy behavior. These dynamics reflect architectural constraints on global routing rather than absence of Bayesian computation, consistent with the separation of static and dynamic geometry we observe.

*Constrained belief-update theories.* The constrained-belief-update model of early-layer attention [1] predicts that attention patterns should stabilize early, while finer-grained posterior refinements should occur in value representations. This matches precisely the frame-precision dissociation predicted in Paper II and observed empirically here: keys define a stable hypothesis frame, while values encode uncertainty refinement along low-dimensional axes.

*Architectural normalization and geometric structure.* Normalization layers and architectural components influence geometric clarity. Recent analyses [2] show that layer normalization, RoPE embeddings, and GQA induce characteristic patterns of anisotropy and dimensionality in the residual stream. Our results refine this picture by showing that such architectural choices modulate *dynamic* signatures (especially attention entropy reduction) while leaving the *static* Bayesian geometry - value manifolds and orthogonal key frames - largely intact.

*Relation to circuit-level interpretability.* Circuit-level analyses [8, 10] identify specific mechanisms such as induction heads, pattern-matchers, and copy circuits. Our work operates at a complementary scale: we provide a geometric account of the global representational substrate in which such circuits operate. Attention mechanisms determine which evidence is consulted; key frames define separable hypothesis directions; and value manifolds encode uncertainty along low-dimensional coordinates. Mapping specific circuits onto these global geometric structures is a promising direction for future work. Overall, the Bayesian geometric lens developed in this series complements prior interpretability approaches by identifying a stable, architecture-spanning substrate for uncertainty representation and by revealing how posterior refinement depends on architectural routing. This perspective helps unify diverse observations in interpretability, probabilistic inference, and model analysis within a single geometric framework.

## 8 Conclusion

This trilogy establishes a unified account of Bayesian inference in neural sequence models:

- **Paper I** shows *which* architectures can implement Bayesian inference, taxonomized by three inference primitives: belief accumulation, belief transport, and random-access binding. Transformers realize all three; Mamba realizes two; LSTMs realize only accumulation of static sufficient statistics; MLPs realize none.

- **Paper II** shows *how* gradient descent learns to implement these primitives through dynamics exhibiting a mechanistic analogy to EM, sculpting a characteristic geometry: low-dimensional value manifolds, orthogonal key frames, and progressive attention focusing.
- **This paper** shows that the geometric substrate for the inference primitives *persists at scale*. Across four model families, we find the same value-manifold structure, key orthogonality, and domain-specific collapse that wind-tunnel models exhibit.

Our analysis shows that large language models organize value vectors along a dominant axis that tracks predictive entropy, keys remain close to orthogonal frames, and domain restriction reliably collapses value manifolds into the same low-rank forms observed in synthetic experiments. This persistent geometric invariant appears across architectures and training regimes, revealing a structural inductive bias toward representing inference geometrically, even in the absence of any explicit Bayesian objective. Our causal probes refine the mechanistic picture. Interventions that remove or perturb the entropy-aligned axis selectively disrupt the local geometry of uncertainty, while matched random interventions do not. Yet these manipulations do not proportionally degrade Bayesian-like behavior, implying that no single direction is solely responsible for the computation. The geometric manifold functions as a stable *readout* of a distributed inference process rather than a brittle circuit. The primitives framework from Paper I explains what capabilities each architecture has; the dynamics from Paper II explain how these capabilities are learned; and this paper establishes that the resulting geometry persists even when the training data lacks ground-truth posteriors. Together with controlled wind-tunnel verification of exact Bayesian inference and gradient-level explanations of its emergence, these results complete a three-part account of existence, mechanism, and persistence at scale. Content-based value routing is not merely sufficient for Bayesian inference—it is a stable representational bias induced by modern transformer architectures and training.

## References

- [1] Naman Agarwal, Siddhartha R. Dalal, and Vishal Misra. 2025. Gradient Dynamics of Attention: How Cross-Entropy Sculptures Bayesian Manifolds. *arXiv:2512.22473* [cs.LG] <https://arxiv.org/abs/2512.22473> Paper II of the Bayesian Attention Trilogy.
- [2] Jimmy Lei Ba, Jamie Ryan Kiros, and Geoffrey E Hinton. 2016. Layer Normalization. *arXiv preprint arXiv:1607.06450* (2016).
- [3] Nora Belrose, Zach Furman, Logan Smith, Danny Halawi, Igor Ostrovsky, Lev McKinney, Stella Biderman, and Jacob Steinhardt. 2023. Eliciting Latent Predictions from Transformers with the Tuned Lens. *arXiv preprint arXiv:2303.08112* (2023).
- [4] Stella Biderman, Hailey Schoelkopf, Quentin Gregory Anthony, Herbie Bradley, Kyle O’Brien, Eric Hallahan, Mohammad Aflah Khan, Shivanshu Purohit, USVSN Sai Prashanth, Edward Raff, et al. 2023. Pythia: A suite for analyzing large language models across training and scaling. *International Conference on Machine Learning* (2023), 2397–2430.
- [5] Tom B. Brown, Benjamin Mann, Nick Ryder, Melanie Subbiah, Jared D. Kaplan, Prafulla Dhariwal, et al. 2020. Language Models are Few-Shot Learners. *Advances in Neural Information Processing Systems* 33 (2020), 1877–1901.
- [6] Mark Chen, Jerry Tworek, Heewoo Jun, Qiming Yuan, Henrique Ponde de Oliveira Pinto, Jared Kaplan, Harri Edwards, et al. 2021. Evaluating Large Language Models Trained on Code. *arXiv preprint arXiv:2107.03374* (2021).
- [7] Kevin Clark, Urvashi Khandelwal, Omer Levy, and Christopher D. Manning. 2019. What Does BERT Look At? An Analysis of BERT’s Attention. In *Proceedings of the 2019 ACL Workshop BlackboxNLP*. 276–286.
- [8] Nelson Elhage, Neel Nanda, Catherine Olsson, Tom Henighan, Nicholas Joseph, Ben Mann, et al. 2021. A Mathematical Framework for Transformer Circuits. Transformer Circuits Thread, Anthropic. <https://transformer-circuits.pub/2021/framework/index.html>
- [9] Nelson Elhage, Neel Nanda, Catherine Olsson, Tom Henighan, Nicholas Joseph, Ben Mann, Amanda Askell, Yuntao Bai, Anna Chen, Tom Conerly, Nova DasSarma, Dawn Drain, Deep Ganguli, Zac Hatfield-Dodds, Danny Hernandez, Andy Jones, Jackson Kernion, Liane Lovitt, Kamal Nduousse, Dario Amodei, Tom Brown, Jack Clark, Jared Kaplan, Sam McCandlish, and Chris Olah. 2021. A Mathematical Framework for Transformer Circuits. Transformer Circuits Thread, Anthropic. <https://transformer-circuits.pub/2021/framework/index.html>

- [10] Catherine Olsson, Nelson Elhage, Neel Nanda, Nicholas Joseph, Nova DasSarma, et al. 2022. In-Context Learning and Induction Heads. Transformer Circuits Thread, Anthropic. <https://transformer-circuits.pub/2022/in-context-learning-and-induction-heads/index.html>
- [11] Catherine Olsson, Nelson Elhage, Neel Nanda, Nicholas Joseph, Nova DasSarma, Tom Henighan, Ben Mann, Amanda Askell, Yuntao Bai, Anna Chen, Tom Conerly, Dawn Drain, Deep Ganguli, Zac Hatfield-Dodds, Danny Hernandez, et al. 2022. In-Context Learning and Induction Heads. Transformer Circuits Thread, Anthropic. <https://transformer-circuits.pub/2022/in-context-learning-and-induction-heads/index.html>
- [12] OpenAI. 2024. OpenAI o1: A New Class of Reasoning Models. *OpenAI Technical Report* (2024).
- [13] Adam S. Shai, Sarah E. Marzen, Lucas Teixeira, Alexander Gietelink Oldenziel, and Paul M. Riechers. 2024. Transformers Represent Belief State Geometry in Their Residual Stream. *Advances in Neural Information Processing Systems* 37 (2024). arXiv:2405.15943.
- [14] Elena Voita, David Talbot, Fedor Moiseev, Rico Sennrich, and Ivan Titov. 2019. Analyzing Multi-Head Self-Attention: Specialized Heads Do the Heavy Lifting, the Rest Can Be Pruned. In *Proceedings of the 57th Annual Meeting of the Association for Computational Linguistics*. 5797–5808.